# Low Complexity Detector Based on Geometric Approximation for the Differential Schemes of Generalized Spatial Modulation

**Deepak Jose** ( deepak.jose@alumni.iitd.ac.in )
Christ University https://orcid.org/0000-0003-3181-5109

**Research Article**

**Keywords:** Spatial modulation (SM), generalized spatial modulation (GSM), differential spatial modulation (DSM), low complexity detector

**Posted Date:** May 18th, 2022

**DOI:** https://doi.org/10.21203/rs.3.rs-1635111/v1

# Low Complexity Detector Based on Geometric Approximation for the Differential Schemes of Generalized Spatial Modulation

Deepak Jose[1*] and Sameer S. M[2†]

[1*]Department of Electronics and Communication Engineering, Christ University, Bangalore, 560074, India.
[2]Department of Electronics and Communication Engineering, National Institute of Technology Calicut, Calicut, 673601, India.

*Corresponding author(s). E-mail(s): deepak.jose@alumni.iitd.ac.in;
Contributing authors: sameer@nitc.ac.in;
†These authors contributed equally to this work.

**Abstract**

Generalized spatial modulation (GSM) has come up as a spectrally efficient transmission scheme for high data rate applications as the information bits are transmitted in multiple dimensions by the selective activation of the transmit antennas, unlike the conventional schemes employing phase and amplitude-based modulations alone. Differential schemes for modulation are essential for receivers having strict energy and processing power constraints since these schemes do not require frequent channel estimation at the receiver. Differential schemes for GSM improves the spectral efficiency in comparison with conventional differential schemes for spatial modulation (SM) with only a nominal increase in the number of transmit antennas. However, ML-based detectors require intensive processing at the receiver. In this paper, a simplified detector based on geometric approximation of the received signal is proposed for the differential schemes of GSM. Firstly, the two-stage detector selects a reduced set of candidates for the transmit antenna combinations based on the correlation with the received signal. A joint detection is performed with the $\boldsymbol{\ell_2}$-norm minimization

approach, on the reduced sets of antenna combinations, along with the modulated symbols lying in the vicinity of the dominant eigenvector of the received signal, to detect the transmitted symbol. The proposed detector has a significant reduction in complexity along with a comparable error performance with respect to the optimal detector.

**Keywords:** Spatial modulation (SM), generalized spatial modulation (GSM), differential spatial modulation (DSM), low complexity detector

# 1 Introduction

One of the challenges of next-generation mobile communication is to ensure a balanced trade-off between the wireless systems spectral efficiency (SE) and energy efficiency (EE) [1]. The existing technologies based on multiple input multiple output (MIMO), is unable to achieve EE using minimum hardware resources since MIMO is designed primarily for high rate transmissions without much focus on reducing the hardware redundancy. The existing communication systems employ dedicated radio frequency (RF) chains at the transmitter to drive every antenna. These RF chains contain different types of power amplifiers (PA), which consume up to 65% of the transmitter circuitry power [2]. Most of the current PA are inefficient since they are unable to operate linearly and close to 80 to 90% of the power is wasted as heat in the PA and they, in turn, require air conditioners, which increases the energy requirements of the base stations (BS) [3].

Spatial modulation (SM) has come up as a transmission scheme, that can dispense with the redundant hardware such as multiple RF chains that are part of existing MIMO-based communication systems [4]. SM can help in reducing the need for multiple RF chains at the transmitter hardware by sharing one RF chain among all the transmit antennas. Also, studies conducted using the Energy Aware Radio and neTwork tecHnology (EARTH)-based power model has shown that BS employing SM are 67% more efficient than the ones using conventional schemes such as multiple input single output (MISO), MIMO and space-time block codes (STBC) in femto, pico, micro and macro cells [5]. It is a priority for mobile operators to keep their costs at a minimum to maintain profitability, and at the same time, they should satisfy the growing data traffic demands in wireless cellular networks [1]. By leveraging the inherent multi-antenna features of MIMO to achieve high rate transmission along with minimum energy and hardware requirement of the SM scheme, future communication systems can achieve the desired performance of a green and cost-effective communication system.

Despite the low energy requirements and low complexity implementation of SM, there is still scope for further improvement at the receiver side, where the maximum likelihood (ML) detectors can be replaced by sub-optimal decoders with lower detection complexity. This is relevant in the context of massive

MIMO which supports large data rates through the multiple data streams transmitted through each of the antennas, and ML detectors become computationally intractable in such scenarios, owing to the large symbol map [6]. The simplest of the detectors for MIMO systems starting with an increase in the order of complexity are the linear detectors such as zero-forcing (ZF) and minimum-mean-square error (MMSE) followed by the sphere decoders (SD) of [7], [8] and [9]. Even though sphere decoders reduce the detection complexity and have a near-optimal performance in most of the channel conditions, they suffer from the initial radius problem and their worst-case complexity is higher. Geometric decoding (GD) is designed to limit such worst-case complexity to a reasonable upper limit in bad channel conditions [10, 11]. Here the search is performed along the dominant direction of the received signal to obtain a reduced set of modulated symbols.

A look into the detection techniques for spatial modulation and its variants such as space shift keying (SSK) [12], generalized SM (GSM)[13], [14] and quadrature SM (QSM) [15] shows that a lot of work focuses on low complexity algorithms for coherent transmission schemes. This is partly because coherent schemes transmit pilot symbols at periodic intervals so that the receivers can perform channel estimation (CE). These estimated channel coefficients available at the start of every frame can be reused for decoding all the information carrying symbols of the same frame, thereby reducing the receiver complexity to some extent. SM is suitable for detection based on sparse signal theory since the symbols have non-zero entries only at a few locations in the symbol matrix. Some of the sub-optimal detectors for SM having reduced computational complexity, is implemented based on the sparse signal theory concepts such as compressive sensing (CS) [16–18], Euclidean-distance based matching pursuit [19] and basis pursuit denoising (BPDN) [20]. Sphere decoders and their improved forms are also implemented for SM to further improve the detection complexity and they have helped in providing near-optimal error performance [21, 22] and [23].

Differential modulation schemes for SM are essential for rapidly varying channel conditions and in user equipments (UE) that cannot afford higher complexity, since these schemes can work without frequent CE at the receiver. Most of the coherent SM schemes rely on the simplifying assumption of perfect-channel state information (P-CSI), and these systems cannot be directly compared with the differential SMs, since the overhead due to the frequent pilot symbols are not factored in and consequently the well-known 3 dB penalty of the differential systems [24] is sometimes an overstatement. It can be seen that the variants of differential spatial modulation (DSM) with a proper design of the encoding strategy could overcome the above penalty in a wide range of signal-to-noise ratio (SNR) [25–27] and [28]. To further reduce the complexity at the receiver, simple detection algorithms are essential for DSM systems and several algorithms are proposed in [29–32] based on the hard-limiting ML approach, Viterbi decoding and CS principles. Amplitude phase shift keying based DSM (APSK-DSMs) [33], [34] improved the SE compared to DSM, and

their detection complexity is further reduced through the algorithms given in [35]. The unified DSM (UDSM) [36] offered flexibility by trading off with the rate-diversity order while designing the symbols. Differential quadrature SM (DQSM) [37] is designed to be spectrally efficient in the lower modulation order, and since it cannot support higher modulation order, they are not suitable for systems with higher data rates. Moreover, the matrix-based symbols employed by most of the DSM schemes create a very large symbol map for an incremental change in the SE, and consequently a larger search space as well. Almost all of these schemes have ML-based detectors alone to perform the decoding and they are not suitable for UEs with limited processing capabilities requiring higher SE at times. Rectangular DSM (RDSM) [26] is an exception to the square matrix-like symbol structure common to the DSM schemes. In RDSMs the rate-diversity factor can be designed with reasonable flexibility. Low complexity detectors for RDSM is proposed in [27], but like other differential schemes for SM, RDSM is also unable to utilize the amplitude domain to improve the spectral efficiency.

Almost all the differential SMs discussed so far employed a single active antenna in a time instant to transmit the modulated symbol, until the works of differential schemes for GSMs (D-GSM) in [28], where multiple antennas are activated at the same time instant to improve the SE. Also, these single active antenna schemes make use of the amplitude domain modulation to improve the SE, similar to the differential schemes such as APSK-DSMs and GD-SM. D-GSM schemes overcame the well-known penalty in SNR with its coherent counterparts and narrowed it down to just 1 dB when compared to the GSM schemes [13] and [14] that employ P-CSI. Even though these schemes reduce the complexity to decode modulated symbols compared with the earlier differential schemes using ML detector, a higher order system always demands a simpler decoding strategy to support mobile UEs having energy and processing power constraints.

In this paper, we present low complexity detection techniques for the two transmission schemes given in [28], using the correlation between the reference symbols and the received information symbols to create a candidate list of transmit antenna combinations (TAC) based on a matching pursuit logic. Then the singular vectors and values obtained using singular value decomposition (SVD) performed on the reference symbols are used to create a reduced set of modulated symbols lying close to the direction of the dominant eigen vector. The contributions of this paper are summarized as follows:

- Proposed low complexity detectors for the differential GSM schemes using a two-stage detection process, where a reduced set of TAC candidates are found out and then by performing a search in the dominant direction to find the most suitable modulated symbol.
- Analyzed the detection complexity of the proposed schemes and compared with the optimal detectors.
- The error performance of the proposed detectors is quantified and it is compared extensively with that of the optimal detectors.

The remainder of this paper is organized as follows: Section 2 describes the system model of the existing SM schemes along with their optimal detectors. The proposed low complexity techniques and the concept of geometric approximation are presented in Section 3. The computational complexities of the proposed detection schemes are analyzed in Section 4. Results of extensive simulation studies are presented in Section 5 followed by the conclusion in Section 6.

*Notations:* We use boldface upper and lower case letters to represent matrices and vectors. The transpose, Hermitian, pseudo-inverse, $\ell_p-$norm and absolute value operations on a vector or matrix are denoted by $(.)^T$, $(.)^H$, $(.)^\dagger$, $\|.\|_p$ and $.$ respectively. $\lfloor . \rfloor$ represents the floor operation and $\binom{\cdot}{\cdot}$ represents the binomial coefficient. The number of transmitter and receiver antennas are denoted by $M_t$ and $M_r$. To represent the number of active antennas in a given time instant $M_u$ is used and $M$ denotes the modulation order of the quadrature amplitude modulation (QAM) or phase shift keying (PSK) constellation. Real or complex numbers are denoted by $\mathbb{R}$ and $\mathbb{C}$, respectively.

# 2 System Models

In this section, we briefly review the multi-antenna differential schemes, D-GSM and differential-multi GSM (D-MGSM) of [28] along with the coherent GSM [13] and [14] to better understand the technique followed in the proposed detection algorithm. The mathematical background required for geometric approximation is also introduced.

## 2.1 Conventional GSM

The first spatial modulation scheme that employed multiple active antennas at a time to transmit the information is proposed in [13], where the system has $M_t$ transmitter antennas, of which $M_u$ number of antennas are active at a time, by sharing the same RF chain. Whereas, the scheme in [14] improved the SE by utilizing the active antennas to transmit unique modulation symbols with the help of dedicated RF chains. Thus the transmitted symbol is represented as $\mathbf{x} = \{0 \dots x_1 \dots 0\, x_{M_u} \dots\}^T$, and the received symbol $\mathbf{y} \in \mathbb{C}^{M_r \times 1}$ is written in general form as,

$$\begin{aligned} \mathbf{y} &= \mathbf{H}\mathbf{x} + \mathbf{n} \\ &= \sum_{i=1}^{M_u} \boldsymbol{h}_{l_i} x_i + \mathbf{n} \end{aligned} \tag{1}$$

where $\boldsymbol{h}_{l_i}$ is the $l_i^{th}$ column of the fading channel matrix $\mathbf{H} \in \mathbb{C}^{M_r \times M_t}$ and $\mathbf{n} \in \mathbb{C}^{M_r \times 1}$ is the additive white Gaussian noise (AWGN) vector.

## 2.2 Differential schemes for GSM

In the schemes presented in [28], multiple active antennas are used to transmit the information, unlike the single active antenna scenario of conventional differential SMs. During the bit mapping of these schemes, the first part of the given bits map to a specific TAC and the rest of the bits are mapped to QAM or PSK symbols and transmitted from each of the active antennas. The schemes differ in the number of RF chains, where D-MGSM requires multiple chains in comparison to the single RF chain of D-GSM. Given below is an example of a transmitter with $M_t = 5$ antennas using $M_u = 2$ active antennas at a time to achieve the information mapping shown in Table 1. Both the schemes have

**Table 1**: Mapping rule of information bits to transmit antenna for D-GSM and D-MGSM

| Information bits | 000 | 001 | 010 | 011 | 100 | 101 | 110 | 111 |
|---|---|---|---|---|---|---|---|---|
| $\mathbb{L}$, Transmit antenna combination | 1, 2 | 1, 3 | 1, 4 | 1, 5 | 2, 3 | 2, 4 | 2, 5 | 3, 4 |

the frame structure given in Figure 1, consisting of $M_t$ reference symbols followed by $K$ normal symbols carrying information. The reference symbol $s^r$ is sent across the transmit antennas during the start of the frame at high power. The reference symbol block received during the start of the frame is given by

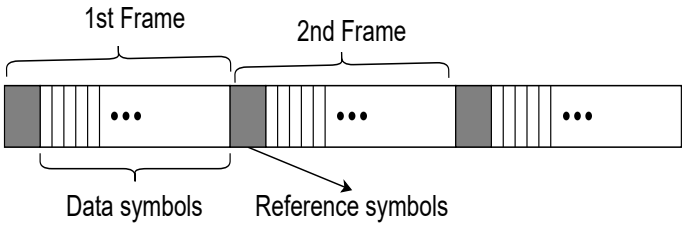


**Fig. 1**: Frame structure of differential GSM schemes

$$\mathbf{Y}^r = \mathbf{H}^r s^r + \mathbf{N}^r. \tag{2}$$

where the entries of the channel fading matrix $\mathbf{H}^r \in \mathbb{C}^{M_r \times M_t}$ and the AWGN matrix $\mathbf{N}^r \in \mathbb{C}^{M_r \times M_t}$, are independent and identically distributed (i.i.d) as $\mathcal{CN}(0, 1)$, $\mathcal{CN}(0, \sigma_r^2)$ respectively. A normal information carrying symbol is encoded as $\mathbf{x}^{(k)} = \{0 \ldots x_1^{(k)} \, x_i^{(k)} \ldots 0 \, x_{M_u}^{(k)} \ldots 0\}^T$, where the non-zero elements correspond to the active antennas, and $x_i^{(k)} \in \mathbb{C}$ is the modulated symbol. The symbol is differentially encoded as

$$\mathbf{s}^n = s^r \mathbf{x}^{(k)} \tag{3}$$

where $s^r$ is the reference signal and $\mathbf{y}^n \in \mathbb{C}^{M_r \times 1}$ is the received signal denoted by

$$\begin{aligned} \mathbf{y}^n &= \mathbf{H}^n \mathbf{s}^n + \mathbf{n}^n \\ &= \sum_{i=1}^{M_u} \boldsymbol{h}_{l_i}^n s^r x_i^{(k)} + \mathbf{n}^n \end{aligned} \tag{4}$$

where $\mathbf{h}_{l_i}^n$ is the column vector of the channel matrix $\mathbf{H}^n \in \mathbb{C}^{M_r \times M_t}$ and $\mathbf{n}^n \in \mathbb{C}^{M_r \times 1}$ is the AWGN vector, whose entries are i.i.d with distribution $\mathcal{CN}(0, 1)$ and $\mathcal{CN}(0, \sigma_n^2)$ respectively. The optimal detector is given by

$$\begin{aligned} [\hat{\mathbb{L}_t}, \hat{x}_i^{(k)}] &= \arg \min_{\forall x_i^{(k)} \in \mathcal{G}, \forall \mathcal{L}} \boldsymbol{y}^n - \sum_{i=1}^{M_u} \boldsymbol{y}_{l_i}^r x_i^{(k)} {}_F^2 \\ &= \arg \min_{\forall x_i^{(k)} \in \mathcal{G}, \forall \mathbb{L}_t \in \mathcal{L}} \mathbf{y}^n - \mathbf{Y}_{\mathbb{L}_t}^r \tilde{\mathbf{x}}^{(k)} {}_F^2 \end{aligned} \tag{5}$$

where $\hat{\mathbb{L}}_t = [l_1, l_2, \ldots, l_{M_u}]$, and it belongs to the TAC set given by $\hat{\mathbb{L}}_t \in \mathcal{L}$, and $\tilde{\mathbf{x}}^{(k)} \in \mathbb{C}^{M_u \times 1}$ contains the non-zero entries of $\mathbf{x}^{(k)}$. This TAC set consists of $\{\mathbb{L}_1, \mathbb{L}_2, \ldots \mathbb{L}_t, \ldots \mathbb{L}_N\}$, such that $N = 2^{\left\lfloor log_2 \binom{M_t}{M_u} \right\rfloor}$ is the total number of valid antenna combinations used for actual transmission and $x_i^{(k)}$ is the amplitude and phase modulated symbol from the symbol map $\mathcal{G}$.

## 2.3 Mathematical preliminaries

The mathematical background required for understanding the geometric approximation is introduced in this section.

1. The SVD of $\mathbf{A} = \mathbf{U}\Sigma\mathbf{V}^H$, where $\mathbf{A} \in \mathbb{C}^{m \times n}$, and the left and right singular vectors are given in the columns of $\mathbf{U}$ and $\mathbf{V}$ respectively. The diagonal matrix $\Sigma$ contains the singular values $\sigma_r$ arranged in the decreasing order of their magnitude as $\sigma_1 \geq \sigma_2 \geq \ldots \sigma_r, \geq \ldots \sigma_p$, where $p = min\{m, n\}$. The right singular vectors corresponding to the above given singular values are ordered as $\mathbf{v}_1, \mathbf{v}_2, \ldots, \mathbf{v}_r \ldots \mathbf{v}_p$ [38].
2. The positive definite matrix $\mathbf{P} = \{\mathbf{A}^H \mathbf{A}\}^{-1} \succcurlyeq 0$ can also be written using the singular vectors of $\mathbf{V}$ as

$$\mathbf{P} = \mathbf{V}\Sigma^{-2}\mathbf{V}^H \tag{6}$$

If $\mathbf{x} \in \mathbb{C}^{n \times 1}$ is a variable, then

$$f(x) = (\mathbf{x} - \mathbf{x}_0)\mathbf{P}(\mathbf{x} - \mathbf{x}_0)^H \leq a^2 \tag{7}$$

is the equation of a hyperellipsoid whose semi-axes is given by the set $\{\mathbf{v}_r\}$, $a \in \mathbb{R}$ and $\mathbf{x}_0 \in \mathbb{C}^{n\times 1}$ is the centre of the hyperellipsoid [39].

3. The condition number of $\mathbf{A}$ is now given by $C_h = \frac{\sigma_p}{\sigma_1} \geq 1$, which indicates the spread or the stretch of the hyperellipsoid formed using the positive definite matrix $\mathbf{A}$. If $C_h >> 1$, and if $n = 2$ then the hyperellipsoid shall be an ellipse in the Euclidean geometry and it shall have the form given in Figure 2.

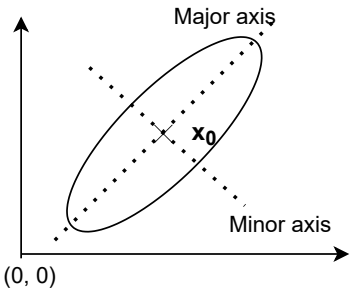


**Fig. 2**: Ellipse skewed in the direction of the major axis

4. In the context of a complex received signal transmitted across a fading channel in the presence of AWGN, the probability density function (pdf) of the signal is given by the contours shown in Figure 3, after applying the $\ell_2$-norm minimization to find the optimal solution. The signal of interest now lies along a specific region and a limited search is only required. A

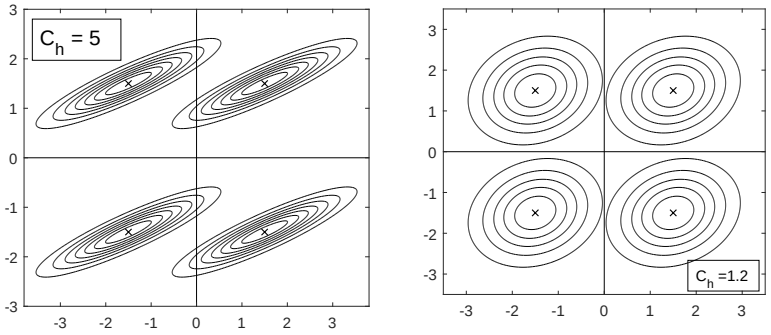


(a) 'Bad' channel, with condition number of $C_h = 5$

(b) 'Good' channel with condition number of $C_h = 1.2$

**Fig. 3**: The pdf of the received QPSK signals after zero forcing equalization in a Rayleigh fading channel with AWGN

well conditioned wireless channel with $C_h \rightarrow 1$, has $\mathbf{H}^H\mathbf{H} \approx \mathbf{I}_{M_t}$ , which

shows that the entries of the channel matrix are uncorrelated, and thus independent fading is guaranteed in the individual channel paths from the transmitter to the receiver.

5. We can write the equation of the line parallel to the major axis of the (hyper) ellipsoid as

$$\mathcal{S}_1 = \{\mathbf{x} | \mathbf{x} = \mathbf{x}_0 + t\mathbf{v}_p\} \tag{8}$$

where $t \in \mathbb{C}$ and the line is offset from the origin by $\mathbf{x}_0$.

# 3 Proposed detection technique

In this section, the different steps involved in the design of the low complexity detector and the techniques required to implement the two-stage detection process are described.

## 3.1 Proposed TAC detection method

The first stage of the low complexity detector involves finding the activated TAC from the received information carrying normal signal using the proposed Algorithm 1, where a candidate list of TAC is formed based on the relation between the different members of the normalized reference signal combination (RSC) map. Since both the transmission schemes involve multiple active antennas during transmission, any two distinct symbols still have a maximum of $M_u - 1$ antennas in common. To estimate the transmitted TAC, the relation between the received normal signal $\mathbf{y}^n$ with all the members of the RSC map is found. The inner product of $\mathbf{y}^n$ with an incorrect RSC member shall produce a maximum of $M_u - 1$ correlated terms. Thus to estimate the transmitted TAC from the correlated terms, it is necessary to create a candidate list of TAC, based on the inner product operation. The condition to include a TAC in the candidate list is decided based on the relation between two distinct RSC. The threshold which decides the candidates in the TAC list is computed by finding the maximum inner product value between the different members of the received reference symbol map where $\mathbf{Y}^r_{\mathbb{L}_p} \in \mathbb{C}_{M_r \times 1}$ is a RSC member having a distinct TAC but $M_u - 1$ common active antennas in comparison with another member $\mathbf{Y}^r_{\mathbb{L}_l} \in \mathbb{C}_{M_r \times 1}$. The relation between two distinct RSC members is computed by $E\left[|\left(\mathbf{Y}^r_{\mathbb{L}_p}\right)^H \mathbf{Y}^r_{\mathbb{L}_l}|\right]$ where the reference symbol member $\boldsymbol{Y}^r_{\mathbb{L}_p}$ and $\boldsymbol{Y}^r_{\mathbb{L}_l}$ contains the combinations of the columns of the reference symbol block $\mathbf{Y}^r = \mathbf{H}^r s_r + \mathbf{N}_r$ given in (2). The relation between the RSC members $\mathbf{Y}^r_{\mathbb{L}_p} = (\sum_{i=1}^{M_u} \boldsymbol{y}^r_{p_i})$ and $\mathbf{Y}^r_{\mathbb{L}_l} = (\sum_{j=1}^{M_u} \boldsymbol{y}^r_{l_j})$ also denotes the number of common active antennas between the members. It is given by

$$\begin{aligned} max\left[|\left(\boldsymbol{Y}^r_{\mathbb{L}_p}\right)^H \boldsymbol{Y}^r_{\mathbb{L}_l}|\right] &= M_u - 1 \\ min\left[|\left(\boldsymbol{Y}^r_{\mathbb{L}_p}\right)^H \boldsymbol{Y}^r_{\mathbb{L}_l}|\right] &= 0 \end{aligned} \tag{9}$$

The relation between the individual constituents of $\mathbf{Y}^r_{\mathbb{L}_p}$ and $\mathbf{Y}^r_{\mathbb{L}_l}$ is given by

$$\begin{aligned} E\left[|\left(\mathbf{y}^r_{p_i}\right)^H \mathbf{y}^r_{l_j}|\right] &= E\left[|\mathbf{y}^r_{q_m}|^2\right] \approx 1, \text{if} p_i = l_j = q_m \\ &= E\left[|\left(\mathbf{y}^r_{p_i}\right)^H \mathbf{y}^r_{l_j}|\right] \approx 0, \text{if} p_i \neq l_j \end{aligned} \tag{10}$$

The value obtained from (9) and (10) is used to fix the tolerance value as $tol = \frac{M_u - 1}{M_u} = 1 - \frac{1}{M_u}$ to create the TAC candidate list, where the maximum value of $M_u$ in the denominator stands for the cardinality value of the RSC member. Each entry of the TAC mapping in Table 1 corresponds to a unique RSC and hence a one-to-one mapping exists between them.

**Algorithm 1** Low complexity algorithm to find the transmit antenna combination

**Init**: RSC map, $\rightarrow \bar{\mathbf{Y}}_{map} = \left[\mathbf{Y}^r_1 \ldots \mathbf{Y}^r_N\right]$, $tol \rightarrow$ Tolerance value to select the RSC candidates.
**Input**: $\mathbf{y}^n$ and $\bar{\mathbf{Y}}_{map}$ the present received signal and reference symbol map in normalized form.
$\mathbf{y_{corr}} = |\bar{\mathbf{Y}}^H_{map} * \bar{\mathbf{y}}^n|$
$[\mathbf{y}^{\mathbf{max}}_{\mathbf{corr}}, i] = max(\mathbf{y_{corr}})$
$\mathbf{y}_{corr}(i) = 0$
**while** $j \leq N$ **do**
    **if** $\mathbf{y}^{\mathbf{max}}_{\mathbf{corr}} - tol \leq \mathbf{y}_{corr}(j)$ **then**
        Include $A_j$ in $\mathcal{L}_C$, the TAC candidate set
        $\mathbf{y}_{corr}(j) = 0$
    **end if**
    $j = j + 1$
**end while**
**Output:** TAC candidate list $\mathcal{L}_C = \{A_1 \ldots A_C\}$. $[\mathbf{u}_c, \sigma_c, \mathbf{v}_c] =$ partial $SVD\left((\mathbf{Y}^r_c)^H * \mathbf{Y}^r_c\right)$

## 3.2 Geometric approximation of the received signal

Geometric approximation for MIMO system [10] is applicable for coherent transmission schemes with constellations having "line-structured" decision regions, such as pulse amplitude modulation (PAM) and square constellations such as 4-QAM, 16-QAM etc. For the D-GSM schemes [28], the optimal detector given in Eq. (5) can be expressed in the form of hyperellipsoids [40], as

$$\begin{aligned} f(\vec{x}) &= (\mathbf{x}^{(k)} - y_{zf})^H \left(\mathbf{Y}^r_{\mathbb{L}}\right)^H \left(\mathbf{Y}^r_{\mathbb{L}}\right) (\mathbf{x}^{(k)} - y_{zf}) \\ &= (\mathbf{x}^{(k)} - y_{zf})^H \mathbf{V} \mathbf{\Sigma}^2 \mathbf{V}^H (\mathbf{x}^{(k)} - y_{zf}) \end{aligned} \tag{11}$$

where $\mathbf{Y}_{\mathbb{L}}^{r} \in \mathbb{C}^{M_r \times M_u}$ corresponds to the RSC and $y_{zf} = \vec{x}_0 = \left(\mathbf{Y}_{\mathbb{L}}^{r}\right)^{\dagger} \mathbf{y}_n$ is the zero-forced received signal. The second part of Eq. (11) is written based on the SVD of $\mathbf{Y}_{\mathbb{L}}^{r} = \mathbf{U}\mathbf{\Sigma}\mathbf{V}^{H}$, and using the singular vectors and values. Thus the postive definite matrix is expressed as $\left(\left(\mathbf{Y}_{\mathbb{L}}^{r}\right)^{H}\left(\mathbf{Y}_{\mathbb{L}}^{r}\right)\right) = \mathbf{V}\mathbf{\Sigma}^{2}\mathbf{V}^{H}$. Now, the auto-correlation of the zero-forced noise $n_{zf} = \left(\mathbf{Y}_{\mathbb{L}}^{r}\right)^{\dagger} \mathbf{n}^{n}$ is given by,

$$\mathbf{R}_{n_{zf}} = \sigma_n^2 \left(\left(\mathbf{Y}_{\mathbb{L}}^{r}\right)^{H}\left(\mathbf{Y}_{\mathbb{L}}^{r}\right)\right)^{-1} = \sigma_n^2 \mathbf{V}\mathbf{\Sigma}^{-2}\mathbf{V}^{H} \tag{12}$$

The real singular values given in $\mathbf{\Sigma}$ is ordered as $\lambda_1 \geq \lambda_2 \geq \ldots \geq \lambda_{M_u}$ and the singular vectors corresponding to these values are given by $\mathbf{v}_1, \mathbf{v}_2, \ldots \mathbf{v}_{M_u}$. The received signal is influenced by the dominant vector of $n_{zf}$, given by $\mathbf{v}_{M_u}$ as inferred from the auto-correlation of (12). Now to find the transmitted signal, the search space is limited to the vicinity of $\mathbf{v}_{M_u}$ and the vector parallel to it is expressed as $\mathcal{S}_1 = \{\vec{\mathbf{x}} | \vec{\mathbf{x}} = \vec{\mathbf{x}}_0 + t\vec{\mathbf{v}}_{M_u}\}$ and in general as, $S_K = \{\vec{\mathbf{x}} | \vec{\mathbf{x}} = \vec{\mathbf{x}}_0 + \mathbf{V}_{\mathcal{K}} t\}$, where $\mathcal{S}_{\mathcal{K}}$ intersects the boundary of a few lattice points out of the entire constellation. The above argument holds true, if the condition number, $C_h = \frac{\lambda_1}{\lambda_{M_u}} >> 1$. In general, the condition number has the value given by $C_h > 10$, and 15 for 32% and 15% of the time the channel is used [10]. The transmitted symbol lies in the vicinity of $\mathcal{S}_{\mathcal{K}}$, as shown in Fig. 3a. Without loss of generality, the complex signal models can be rewritten in real form using suitable transformation of the matrices. The notations $\Re(.)$ and $\Im(.)$ denotes the real and imaginary part of the complex column matrix or matrix and the subscript $r$ denotes the converted real-form representation of the matrix as shown below.

$$\mathbf{x} \rightarrow \mathbf{x}_r = \begin{bmatrix} \Re\{\mathbf{x}\} \\ \Im\{\mathbf{x}\} \end{bmatrix}, \mathbf{M} \rightarrow \mathbf{M}_r = \begin{bmatrix} \Re\{\mathbf{M}\} & -\Im\{\mathbf{M}\} \\ \Im\{\mathbf{M}\} & \Re\{\mathbf{M}\} \end{bmatrix}$$

Now the point of intersection of $\mathcal{S}_1$ with the lattice boundaries is found using the below steps:-

1. Dominant direction, $S_1 = \{\vec{\mathbf{x}} | \vec{\mathbf{x}_r} = \mathbf{x}_{0r} + \mathbf{V}_{r1} t_r\}$
2. $\mathbf{B} = \{B_1, B_2, \ldots, B_{M_{db}}\}$ are the decision boundaries of the constellation.
3. Point of intersection of $S_1$ and $\mathbf{B}$ is given by $t_{n,j} = \mathbf{V}_{r1}{}^{\dagger} * \{B_{rj} - \mathbf{x}_{0r}\}$.
4. Sorting the points of intersection $t_{n,j}$ such that $t_{n,j} \rightarrow t_{(ir)}$, in the order of their distance from the centre $\vec{\mathbf{x}}_0$ is as given by $|t_{(1r)}| \leq |t_{(2r)}| \leq \cdots \leq |t_{(M_u \times M_{db})r}|$.

The constellations near to the above lattice intersections are iteratively checked for their optimality in (11) using Algorithm 2 and the best symbol is chosen.

# 4 Computational Complexity analysis

We have used the total number of complex floating point operations (flops) to quantify the computational complexity of the proposed detectors with the existing ML detectors. Here flops account for the number of complex multiplications and additions required for the detection process. A few steps of the

**Algorithm 2** Geometric approach for finding the M-QAM symbol

1: **Input**: Reduced list of singular vectors and singular values $\mathcal{V}_C = \{\mathbf{V}_{r1} \dots \mathbf{V}_{rC}\}$, $\Sigma_C = \{\sigma_1 \dots \sigma_C\}$. $\mathbf{x}_{0r}$, is the zero forced received signal. $M_{db} \rightarrow$ No. of constellation boundaries. $\epsilon = 0.1$
2: **for** $i = 1$ to $C$ **do**
3: Find points of intersection corresponding to $t_{1r}$ : $\mathbf{x}_{1r}^{\pm} = \mathbf{x}_{0r} + (1 \pm \epsilon)\mathbf{V}_{ri}\mathbf{t}_{1r}$
4: $\tilde{\mathbf{x}}_{1r}^{\pm} = quantiz\left(\mathbf{x}_{1r}^{\pm}\right)_{Q_M}$, to quantize to nearest symbol.
5: $\hat{x}_S = \arg\min\{f\left(\tilde{x}_1^{+}\right), f\left(\tilde{x}_1^{-}\right)\}$
6: $d^2 = \min\{f\left(\tilde{x}_1^{+}\right), f\left(\tilde{x}_1^{-}\right)\}$, Set $j = 2$
7: **while** $t_{jr} \leq \sigma_l d^2$ or $j \leq M_{db} * M_u$ **do**
8: $\mathbf{x}_{jr}^{+} = \mathbf{x}_{0r} + (1 + \epsilon)\mathbf{V}_{ri}\mathbf{t}_{jr}$
9: $\tilde{\mathbf{x}}_{jr}^{+} = quantiz\left(\mathbf{x}_{jr}^{+}\right)_{Q_M}$
10: **if** $f\left(\tilde{x}_j^{+}\right) \leq d^2$ **then**
11: $d^2 = f\left(\tilde{x}_j^{+}\right)$
12: $\hat{x}_S = \tilde{x}_j^{+}$
13: **end if**
14: $j = j + 1$
15: **end while**
16: **end for**

proposed detection process is common for both the schemes and they are computed once during the start of every frame, whereas other computations are performed for each of the $K$ symbols separately. The computations are: (i) the flops corresponding to the partial SVD operation as well as the pseudo-inverse operation [38] of $\left(\mathbf{Y}_{\mathbb{L}}^{r}\right)^{\dagger}$, is given by $N_{svd} = N\left(13{M_u}^3 + 2M_r{M_u}^2 + 2{M_r}^2M_u\right)$, which is computed once and used throughout a frame (ii) The flops invoved in the computation of the intersection points with the lattice boundaries is given by $3KM_{db}M_u$. (iii) The correlation operation with the received signal in Algorithm 1, to find the TAC candidate list requires a total of $2KM_tM_r$ flops. (iv) When the iterative search operation in Algorithm 2 yields a selected few candidates of $\tilde{\mathbf{x}}_{jr}^{\pm}$ given in step 8, the total associated flops is given by $KN_pD_{int}^{avg}(2M_u + M_r)$. Here $N$ is the is the total number of valid antenna combinations defined in Section 2.2, $K$ is the total number of data symbols in a frame. $D_{int}^{avg}$ refers to the average number of intersections of the singular vector with the constellation boundaries and the possible number of intersections with the given constellation lies in the range $D_{int} \in [1, M_u(M-2)+1]$ for 4-QAM and $D_{int} \in [1, M_u(M-10)+1]$ for 16-QAM. $D_{int}^{avg}$ is found to be 3 and 7 for the 4-QAM and 16-QAM constellations using $M_u = 2$ antennas. $N_p = C$ is the average number of TACs in the candidate list and $M_{db}$ refers to the number of decision boundaries for the given constellation such that $M_{db} = 2, 6$ for 4-QAM and 16-QAM respectively. The operations related to the steps (ii), (iii) and (iv) which are required to find the TAC candidate list and

the intersection points corresponding to a single symbol is combined as given by $N_{tac\_intr} = 3KM_{db}M_u + KN_pD_{int}^{avg}(2M_u + M_r) + 2KNM_r$. The rest of the operations are specific to the proposed detector for D-GSM which is given by $MNM_r(2M_u - 1)$, and it corresponds to all the possible combinations of the RSC with the constellation symbol given by $\sum_{i=1}^{M_u} \mathbf{y}_{l_i}^r \hat{x}_i^{(k)}$ in (5). The computations required for the proposed detector is given below along with the computations required for the ML detector corresponding to the D-GSM scheme.

$$C_{ml} = MN\,(2M_rM_u - M_r + K(3M_r - 1)) \tag{13}$$

$$C_{proposed} = N_{svd} + N_{tac\_intr} + MNM_r(2M_u - 1) \tag{14}$$

where the flops for the $K$ symbols in a frame is also accounted for. In Fig. 4, the computations required for various system configurations of the D-GSM scheme are given for $M_u = 2$. We can observe a 30 to 80% reduction in complexity compared to the optimal detector, as the order of the system increases. The reduction in complexity is computed with respect to the ML scheme as given by,

$$\%Reduction = \frac{100 \times \left(C_{ml} - C_{proposed}\right)}{C_{ml}} \tag{15}$$

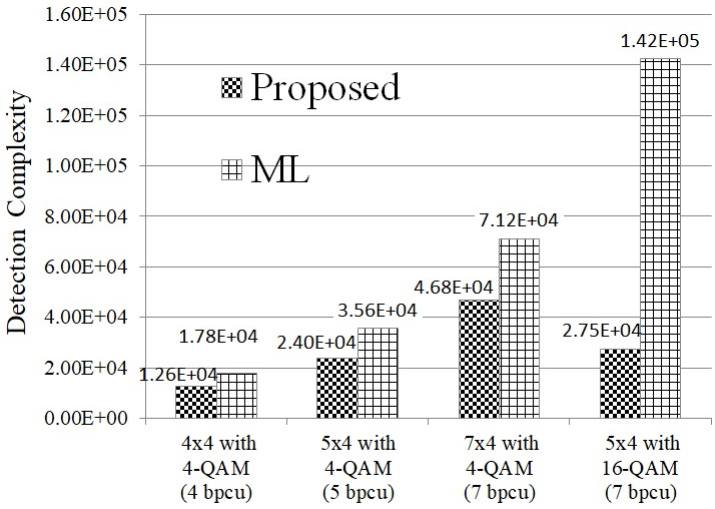


**Fig. 4**: Complexity of the ML detectors for D-GSM scheme along with the proposed detector for different $M_t \times M_r$ configurations

The complexity calculations of the proposed detector for D-MGSM includes steps (i), (ii), (iii) and (iv) as given above. These are the flops required for the SVD calculations and for finding the points of intersection of the dominant vector with the constellation boundaries. In addition to the above, D-MGSM

detector requires $2^{M_u} MNM_r(2M_u - 1)$ flops as well, for the $\mathbf{y}_{l_i}^r \hat{x}^{(k)}$ operation which is performed $M_u$ times and stored at the start of every frame. The associated flops are given by

$$C_{ml} = 2^{M_u} MN\,(2M_r M_u - M_r + K\,(3M_r - 1)) \tag{16}$$

$$C_{proposed} = N_{svd} + N_{tac\_intr} + 2^{M_u} MNM_r(2M_u - 1) \tag{17}$$

The comparison of the complexities of the detectors for the D-MGSM scheme is presented in Fig. 5, where we can observe that the proposed detector has a complexity reduction of more than 80%, when compared to the ML detectors for various system configurations. The above results substantiate the assumption that the detection complexity can be brought down if the search is limited to the vicinity of the dominant eigenvector of the channel matrix, unlike the brute-force approach in conventional ML-based detectors, where the complete symbol map is searched to find the optimal symbol.

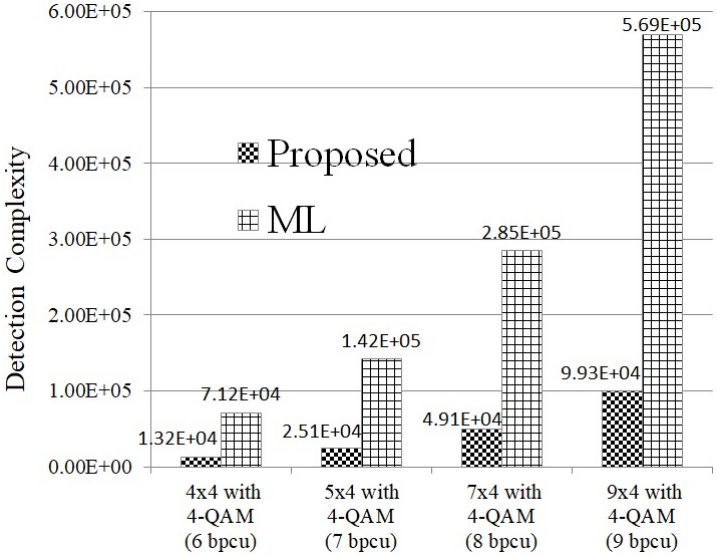


**Fig. 5**: Complexity of the ML detectors for the D-MGSM scheme along with the proposed detector for different $M_t \times M_r$ configurations

## 5 Simulation Studies and Discussion

In this section, we shall compare the error performance of the proposed detectors with the optimal detectors of the D-GSM and D-MGSM schemes [28]. The results are obtained through Monte-Carlo simulations in a block fading Rayleigh channel. For all the investigated cases the average symbol SNR per

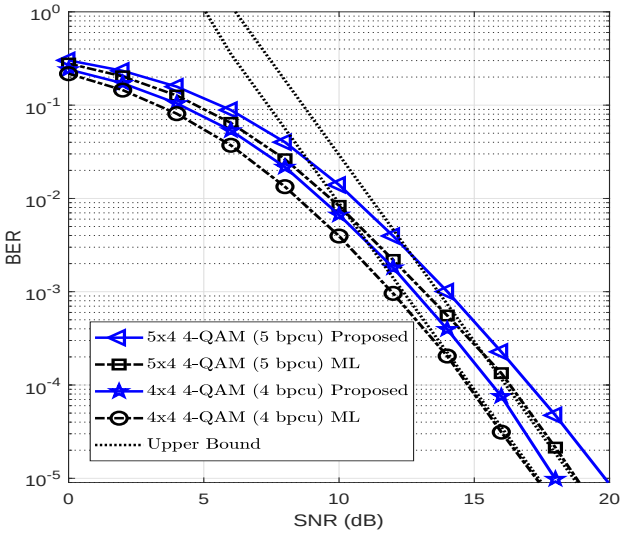


**Fig. 6**: Comparison of BER of the D-GSM scheme using the different detectors in a Rayleigh fading channel

**Table 2**: Simulation Parameters

| | |
|---|---|
| Channel | Rayleigh fading |
| Modulation (M) | 4, 16, MQAM |
| Number of transmit antennas ($M_t$) | 4, 5, 7 |
| Number of receive antennas ($M_r$) | 4 |
| Information symbols per frame ($K$) | 100 |

receive antenna is varied as one of the parameter. Fig. 6 shows that the BER performance of the proposed detector has a marginal penalty of only 1 dB compared with the ML detector for $M_t = 4, 5$. Since square constellations are only considered, the modulation order is chosen as $M = 4, 16$. In Fig. 7, the ML detector for the D-MGSM scheme has a gain of 0.8 dB alone with the proposed detector for the antenna configurations of $M_t = 4, 5$ having a SE of 6 and 7 bpcu. The asymptotic upper bound of the error performance of the optimal detectors is derived in [28] using the moment generating function approach. The comparison of the optimal detector and its upper bound with the proposed detectors of D-GSM and D-MGSM in Fig. 6 and 7 demonstrates the latter having a negligible penalty in error performance. The detectors are also compared at a higher SE of 6, 9 and 10 bpcu in Fig. 8 using $M_t = 7$ transmit antennas using a higher modulation order of $M = 16$. Here the proposed detectors maintain a notable error performance in comparison with the ML detectors.

In general for both the schemes, the performance of the proposed detector is close to the optimal detector for different antenna configurations and close to the upper bound of the error probability from the mid-SNR region onwards

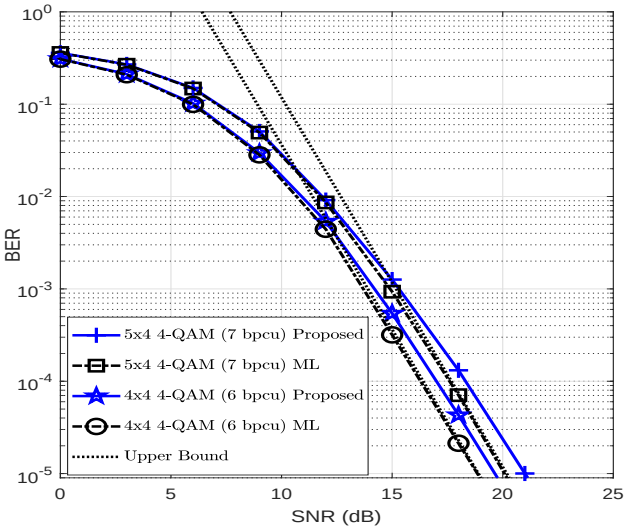


**Fig. 7**: Comparison of BER of the D-MGSM scheme using the different detectors in a Rayleigh fading channel by varying the antenna order

and for the BER of $10^{-2}$ or lesser. When a massive antenna configuration is used, the search space in the dominant direction have to expand to either the two-dimensional or the three-dimensional space to achieve a good detection performance. Nevertheless, the proposed low complexity detection schemes are an alternative for the computationally intensive optimal detectors as seen from their marginal penalty in BER.

# 6 Conclusion

In this paper, we have proposed low complexity detectors for D-GSM and D-MGSM based on the correlation approach to find the TAC candidate list. The constellation symbol is found using the geometrical approximation of the received signal. Even though the proposed detectors have a negligible penalty in error performance when compared with the optimal detectors, their computational complexity is significantly lower than that of the optimal detectors. For a wide range of SE, the proposed detectors are suitable, when the optimal detectors become computationally prohibitive. In general, the proposed detectors favour devices having power and processing limitations without compromising on the error performance by utilizing the inherent channel characteristics, which skew the received signal in a specific direction. These detectors are very relevant in next-generation communication devices with the rising demand for cost-effectiveness and power efficiency towards the goal of green communication systems.

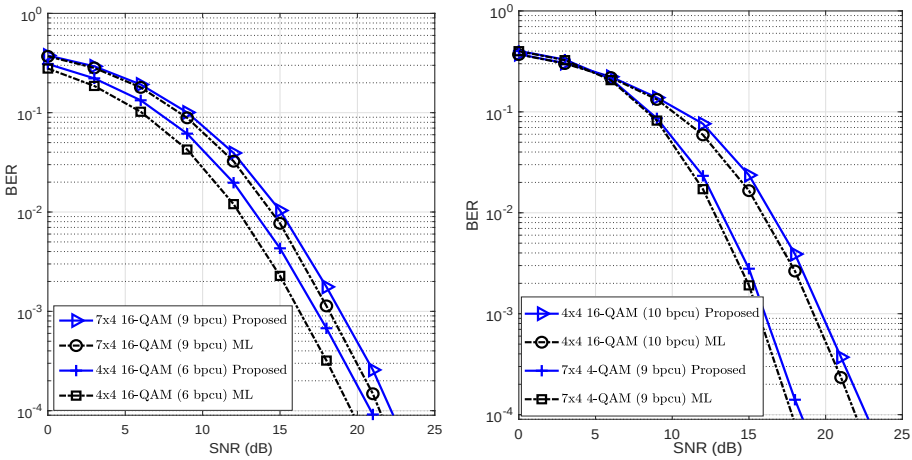


(a) Error performance of the detectors for the D-GSM scheme

(b) Error performance of the detectors for the D-MGSM scheme

**Fig. 8**: Comparison of the error performance of the detectors for higher spectral efficiency using various $M_t \times M_r$ configurations

**Acknowledgments.** Authors would like to thank the Department of Science & Technology, Government of India for supporting this work under the FIST scheme No. SR/FST/ET-I/2017/68

# STATEMENTS AND DECLARATIONS

## Funding

This work has been supported by the Department of Science & Technology, Government of India under the FIST scheme No. SR/FST/ET-I/2017/68

## Competing Interests

The authors have no relevant financial or non-financial interests to disclose. No conflict of interest is involved.

## Author Contributions

All authors contributed to the study conception and design. Material preparation, data collection and analysis were performed by Deepak Jose and Sameer S. M. The first draft of the manuscript was written by Deepak Jose and all authors commented on previous versions of the manuscript. All authors read and approved the final manuscript.

## Code availability

Not applicable.

## Data Availability

The datasets generated during and/or analysed during the current study are available from the corresponding author on reasonable request. The dataset is randomly generated using a general purpose mathematical operation and hence does not have any ownership associated to it.

# References

[1] Renzo, M. D., Haas, H., Ghrayeb, A., Sugiura, S. & Hanzo, L. Spatial modulation for generalized MIMO: Challenges, opportunities, and implementation. *Proc. of the IEEE* **102** (1), 56–103 (2014). https://doi.org/10.1109/JPROC.2013.2287851 .

[2] Deloitte. Telecom predictions 2010 (2014). https://www.slideshare.net/pokamoto/deloitte-telecom-predictions-2010.

[3] Hasan, Z., Boostanimehr, H. & Bhargava, V. K. Green cellular networks: A survey, some research issues and challenges. *IEEE Commun. Surveys Tut.* **13** (4), 524–540 (2011) .

[4] Jeganathan, J., Ghrayeb, A. & Szczecinski, L. Spatial modulation: optimal detection and performance analysis. *IEEE Commun. Lett.* **12** (8), 545–547 (2008). https://doi.org/10.1109/LCOMM.2008.080739 .

[5] Stavridis *et al.* Energy evaluation of spatial modulation at a multi-antenna base station (2013). Proc. of 2013 IEEE 78th Vehicular Technology Conference (VTC Fall) in Las Vegas, NV, USA, Sep. 2013.

[6] Albreem, M. A., Juntti, M. & Shahabuddin, S. Massive mimo detection techniques: A survey. *IEEE Commun. Surveys Tut.* **21** (4), 3109–3132 (2019). https://doi.org/10.1109/COMST.2019.2935810 .

[7] Viterbo, E. & Boutros, J. A universal lattice code decoder for fading channels. *IEEE Trans. Info. Theory.* **45** (5), 1639–1642 (1999). https://doi.org/10.1109/18.771234 .

[8] Agrell, E., Eriksson, T., Vardy, A. & Zeger, K. Closest point search in lattices. *IEEE Trans. Info. Theory.* **48** (8), 2201–2214 (2002). https://doi.org/10.1109/TIT.2002.800499 .

[9] Damen, M., El Gamal, H. & Caire, G. On maximum-likelihood detection and the search for the closest lattice point. *IEEE Trans. Info. Theory.* **49** (10), 2389–2402 (2003). https://doi.org/10.1109/TIT.2003.817444 .

[10] Artes, H., Seethaler, D. & Hlawatsch, F. Efficient detection algorithms for MIMO channels: a geometrical approach to approximate ML detection.

*IEEE Trans. Signal Process.* **51** (11), 2808–2820 (2003). https://doi.org/10.1109/TSP.2003.818210 .

[11] Samuel, M. & Fitz, M. P. Geometric decoding of PAM and QAM lattices (2007). Proc. of IEEE GLOBECOM 2007-2007 IEEE Global Telecommunications Conference in Washington, USA, Nov. 2007.

[12] Renzo, M. D., Leonardis, D. D., Graziosi, F. & Haas, H. Space shift keying mimo with practical channel estimates. *IEEE Trans. Commun.* **60** (4), 998–1012 (2012). https://doi.org/10.1109/TCOMM.2012.021712.100778 .

[13] Younis, A., Serafimovski, N., Mesleh, R. & Haas, H. Generalised spatial modulation (2010). Proc. of Conference Record of the Forty Fourth Asilomar Conference on Signals, Systems and Computers in Pacific Grove, USA, Nov. 2010.

[14] Wang, J., Jia, S. & Song, J. Generalised spatial modulation system with multiple active transmit antennas and low complexity detection scheme. *IEEE Trans. Wireless Commun.* **11** (4), 1605–1615 (2012) .

[15] Mesleh, R., Ikki, S. S. & Aggoune, H. M. Quadrature Spatial Modulation. *IEEE Trans. Veh. Technol.* **64** (6), 2738–2742 (2015). https://doi.org/10.1109/TVT.2014.2344036 .

[16] Yu, C.-M. *et al.* Compressed sensing detector design for space shift keying in MIMO systems. *IEEE Commun. Lett.* **16** (10), 1556–1559 (2012). https://doi.org/10.1109/LCOMM.2012.091212.121319 .

[17] Xiao, L. *et al.* Efficient compressive sensing detectors for generalized spatial modulation systems. *IEEE Trans. Veh. Technol.* **66** (2), 1284–1298 (2017). https://doi.org/10.1109/TVT.2016.2558205 .

[18] Wang, C. *et al.* Near-ML low-complexity detection for generalized spatial modulation. *IEEE Commun. Lett.* **20** (3), 618–621 (2016). https://doi.org/10.1109/LCOMM.2016.2516542 .

[19] Zhang, L., Zhu, S., Zhang, L. & Jin, M. Low-complexity sparse detector for generalised space shift keying. *Electronics Letters* **55** (5), 268–270 (2019). https://doi.org/10.1049/el.2018.7977 .

[20] Liu, W., Wang, N., Jin, M. & Xu, H. Denoising detection for the generalized spatial modulation system using sparse property. *IEEE Commun. Lett.* **18** (1), 22–25 (2014). https://doi.org/10.1109/LCOMM.2013.111413.131722 .

[21] Younis, A., Di Renzo, M., Mesleh, R. & Haas, H. Sphere decoding for spatial modulation (2011). Proc. of 2011 IEEE International Conference on Communications (ICC) in Kyoto, Japan, June 2011.

[22] Rajashekar, R. & Hari, K. V. S. Sphere decoding for spatial modulation systems with arbitrary Nt. *arXiv preprint arXiv:1202.5187* (2013) [cs.IT].

[23] Younis, A., Sinanovic, S., Di Renzo, M., Mesleh, R. & Haas, H. Generalised sphere decoding for spatial modulation. *IEEE Trans. Commun.* **61** (7), 2805–2815 (2013). https://doi.org/10.1109/TCOMM.2013.061013.120547 .

[24] Bian, Y. *et al.* Differential spatial modulation. *IEEE Trans. Veh. Technol.* **64** (7), 3262–3268 (2015) .

[25] Kadathlal, K., Xu, H. & Pillay, N. Generalised differential scheme for spatial modulation systems. *IET Commun.* **11** (13), 2020–2026 (2017). https://doi.org/10.1049/iet-com.2017.0342 .

[26] Ishikawa, N. Rectangular differential spatial modulation for open-loop noncoherent massive-mimo downlink. *IEEE Trans. Wireless Commun.* **16** (3), 13 (2017) .

[27] Xiao, L. *et al.* Differentially-encoded rectangular spatial modulation approaches the performance of its coherent counterpart. *IEEE Trans. Commun.* **68** (12), 7593–7607 (2020). https://doi.org/10.1109/TCOMM.2020.3021117 .

[28] Jose, D. & Sameer, S. M. Differential transmission schemes for generalized spatial modulation. *IEEE Transactions on Vehicular Technology* **70** (12), 12640–12650 (2021). https://doi.org/10.1109/TVT.2021.3118457 .

[29] Xiao, L. *et al.* Low-complexity detection scheme for differential spatial modulation. *IEEE Commun. Lett.* **19** (9), 1516–1519 (2015) .

[30] Wei, R.-Y. & Lin, T.-Y. Low-complexity differential spatial modulation. *IEEE Wireless Commun. Lett.* **8** (2), 356–359 (2019). https://doi.org/10.1109/LWC.2018.2872990 .

[31] Miaowen Wen, Xiang Cheng, Yuyang Bian & Poor, H. V. A low-complexity near-ML differential spatial modulation detector. *IEEE Signal Processing Lett.* **22** (11), 1834–1838 (2015). https://doi.org/10.1109/LSP.2015.2425042 .

[32] Jose, D. & Sameer, S. M. Compressive sensing-based low-complexity detector for differential spatial modulation. *IET Commun.* **13** (19), 3229–3234 (2019). https://doi.org/10.1049/iet-com.2019.0016 .

[33] Martin, P. A. Differential spatial modulation for apsk in time-varying fading channels. *IEEE Commun. Lett.* **19** (7), 1261–1264 (2015) .

[34] Liu, J. *et al.* High-rate apsk-aided differential spatial modulation: Design method and performance analysis. *IEEE Commun. Lett.* **21** (1), 168–171 (2017). https://doi.org/10.1109/LCOMM.2016.2610962 .

[35] Jose, D. & Sameer, S. M. Low complexity detector for amplitude phase shift keying-based differential spatial modulation. *IET Commun.* **14** (20), 3669–3675 (2020). https://doi.org/10.1049/iet-com.2020.0120 .

[36] Ishikawa, N. & Sugiura, S. Unified differential spatial modulation. *IEEE Wireless Commun. Lett.* **3** (4), 337–340 (2014). https://doi.org/10.1109/LWC.2014.2315635 .

[37] Mesleh, R., Althunibat, S. & Younis, A. Differential quadrature spatial modulation. *IEEE Trans. Commun.* **65** (9), 3810–3817 (2017). https://doi.org/10.1109/TCOMM.2017.2712720 .

[38] Golub, G. H. & Van Loan, C. F. *Matrix computations* Fourth edn (The Johns Hopkins University Press, 2013).

[39] Horn, R. A. & Johnson, C. R. *Matrix analysis* 2nd edn (Cambridge University Press, 2012).

[40] Fincke, U. & Pohst, M. Improved methods for calculating vectors of short length in a lattice, including a complexity analysis. *Mathematics of Computation* **44** (170), 463–471 (1985) .

# Supplementary Files

This is a list of supplementary files associated with this preprint. Click to download.

- Authorbiospringer.pdf